Structure
Article

Structure of IL-22 Bound to Its High-Affinity IL-22R1 Chain

Brandi C. Jones,[1] Naomi J. Logsdon,[1] and Mark R. Walter[1,2,*]
[1]Center for Biophysical Sciences and Engineering
[2]Department of Microbiology
University of Alabama at Birmingham, Birmingham, AL 35294, USA
*Correspondence: walter@uab.edu
DOI 10.1016/j.str.2008.06.005

SUMMARY

IL-22 is an IL-10 family cytokine that initiates innate immune responses against bacterial pathogens and contributes to immune disease. IL-22 biological activity is initiated by binding to a cell-surface complex composed of IL-22R1 and IL-10R2 receptor chains and further regulated by interactions with a soluble binding protein, IL-22BP, which shares sequence similarity with an extracellular region of IL-22R1 (sIL-22R1). IL-22R1 also pairs with the IL-20R2 chain to induce IL-20 and IL-24 signaling. To define the molecular basis of these diverse interactions, we have determined the structure of the IL-22/sIL-22R1 complex. The structure, combined with homology modeling and surface plasmon resonance studies, defines the molecular basis for the distinct affinities and specificities of IL-22 and IL-10 receptor chains that regulate cellular targeting and signal transduction to elicit effective immune responses.

INTRODUCTION

Interleukin-22 (IL-22) is an α-helical cytokine produced by activated DC and T cells, including the recently identified Th17 lineage (Dumoutier et al., 2000a; Liang et al., 2006). Despite its production by immune cells, IL-22 biological activity is specifically targeted to cells of epithelial origins, where it induces pro-inflammatory activities that include the production of early systemically circulated defense proteins (acute phase proteins) (Dumoutier et al., 2000b). More recently, IL-22 has been shown to induce antimicrobial proteins, including S100s and defensins, in colonic and lung epithelial cells, which are critical for host defense against enteric and pulmonary bacterial pathogens (Aujla et al., 2008; Liang et al., 2006; Wolk et al., 2004; Zheng et al., 2008). This suggests that IL-22 allows coordination between the adaptive and innate immune systems to fight invading pathogens.

In addition to its pro-inflammatory activities, IL-22 confers a protective effect on the liver by promoting hepatocyte survival (Radaeva et al., 2004; Zenewicz et al., 2007). IL-22 also enhances lung epithelial cell proliferation and the maintenance of trans-epithelial resistance to injury (Aujla et al., 2008). IL-22-mediated protective effects have also been observed in the gut, where IL-22 knockout mice, subjected to *Citrobacter rodentium* infection, exhibit increased epithelial cell damage and increased mortality (Zheng et al., 2008). Thus, IL-22 exhibits paradoxical pro- and anti-inflammatory properties on epithelial cells, which are strikingly similar to the activity profile of IL-10 on immune cells (Moore et al., 2001).

IL-22 and IL-10 induce cellular responses by engaging heterodimeric cell-surface receptor complexes that contain IL-22R1 and IL-10R1 chains, respectively, and the shared signal transducing receptor, IL-10R2 (Figure 1; Kotenko et al., 2001a; Xie et al., 2000). Formation of the IL-22/IL-22R1/IL-10R2 complex activates intracellular kinases (JAK1, Tyk2, and MAP) and transcription factors, especially STAT3, leading to IL-22 cellular responses (Lejeune et al., 2002). IL-10/IL-10R1/IL-10R2 assembly induces overlapping kinases and also predominantly activates STAT3 (Moore et al., 2001).

IL-22R1 is selectively expressed on skin and epithelial cells, whereas IL-10R1 is predominantly expressed on DC cells, monocytes, and macrophages (Nagalakshmi et al., 2004). In contrast, IL-10R2 is expressed on all cell types, which reflects its role as a shared receptor in IL-22, IL-10, IL-26, IL-28, and IL-29 receptor complexes. Surface plasmon resonance (SPR) studies are consistent with the targeting function of IL-22R1 and IL-10R1 (Logsdon et al., 2002, 2004; Yoon et al., 2005, 2006). sIL-22R1 and sIL-10R1 both exhibit high affinity (~nM) for their respective ligands. In contrast, IL-10R2 interactions are very weak (~μM–mM), which may facilitate promiscuous, but essential, interactions in multiple cytokine complexes resulting in cellular signaling responses.

IL-22 and IL-10 are structurally similar to each other and to the rest of the IL-10 cytokine family, which includes IL-19, IL-20, IL-24, and IL-26 (Pestka et al., 2004). In addition to specific high-affinity interactions with IL-22, IL-22R1 also pairs with IL-20R2 to induce IL-20 and IL-24 signaling (Dumoutier et al., 2001a; Figure 1). Like IL-22, IL-20 and IL-24 have been implicated in skin homeostasis and pathology (Blumberg et al., 2001; Kunz et al., 2006; Sa et al., 2007). IL-20 induces keratinocyte proliferation, and overexpression in mice leads to a psoriasis-like phenotype (Blumberg et al., 2001). In contrast to IL-22, IL-20 and IL-24 are expressed predominantly by monocytes and keratinocytes. Under Th1 conditions, IL-22R1 and IL-20R2 chains are also expressed on keratinocytes (Kunz et al., 2006). This suggests that IL-20 and IL-24, via the IL-22R1/IL-20R2 complex, may provide a communication link between monocytes and keratinocytes, as well as a feedback loop on keratinocytes themselves.

The high level of IL-22 in human psoratic plaques and its pathogenic role in a mouse model of psoriasis suggest that

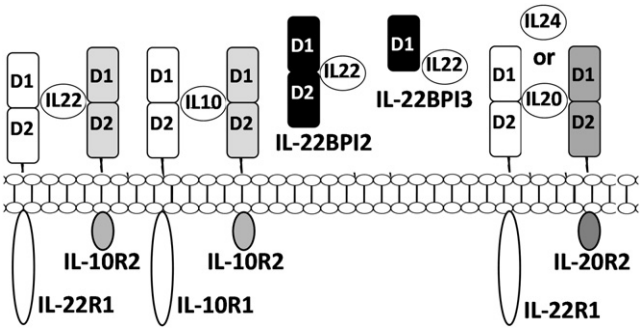

Figure 1. Schematic Diagram of Protein Complexes Formed by IL-22 Receptors

Although not shown, IL-10R2 also forms IL-20R1/IL-10R2 and IL-28R1/IL-10R2 cell-surface complexes that activate IL-26, IL-28, and IL-29 signaling.

antagonists that block the IL-22/sIL-22R1 interaction may have therapeutic potential (Boniface et al., 2007; Ma et al., 2008; Wolk et al., 2006). Furthermore, cells tightly regulate IL-22 activities by expressing an IL-22 binding protein (IL-22BP), which shares 34% sequence identity with the extracellular region of IL-22R1 (sIL-22R1) (Dumoutier et al., 2001b; Kotenko et al., 2001b; Wei et al., 2003; Xu et al., 2001). Three splice forms of human IL-22BP have been identified in human cells (Kotenko et al., 2001b). Mature IL-22BP isoform 2 (IL-22BPI2; SWISS-PROT ID Q969J5-2) is 210 amino acids long and predicted to adopt a structure similar to sIL-22R1, whereas isoform 3 (IL-22BPI3; SWISS-PROT ID Q969J5-3) is 109 amino acids long and should adopt a structure similar to the sIL-22R1 D1 domain (Figure 1). The biochemical properties and functional roles of the IL-22BP isoforms have not been elucidated.

The fidelity of intracellular signaling between innate and adaptive immune systems is critical to balance pathogen elimination versus damage to host tissues. IL-22 and IL-22R1 play critical roles in this process, not only by activation of the IL-22/IL-22R1/IL-10R2 complex, but through additional diverse interactions between IL-22 and IL-22BP and the participation of IL-22R1 in IL-20/IL-22R1/IL-20R2 and IL-24/IL-22R1/IL-20R2 complexes. To understand the molecular basis of these protein/protein interactions, we have determined the structure of the IL-22/sIL-22R1 complex. Comparison of IL-22/sIL-22R1 and IL-10/sIL-10R1 structures, combined with homology modeling and SPR analysis of IL-22/IL-22BP and IL-22/IL-22R1/IL-10R2 complexes, provides a molecular understanding of how these molecules form specific and promiscuous complexes with affinities that differ by approximately six orders of magnitude (Table 1; Figure 1).

RESULTS

Structure Determination

The IL-22/sIL-22R1 structure was solved by single-wavelength anomalous dispersion (SAD) phasing and refined at 2.5 Å resolution to R_{cryst} and R_{free} values of 22.2% and 27.0%, respectively (see Table S1 available online). IL-22 used for crystallization ($IL\text{-}22_{N\text{-}QQ}$) contained no N-linked glycosylation, and sIL-22R1 ($sIL\text{-}22R1_{DDQ}$) contains carbohydrate at one of three sites, Asn-$172^{sIL\text{-}22R1}$ (Jones et al., 2008), which is observed in the structure

Table 1. Binding Constants for IL-22 and IL-10

Complexes	k_{on} ($M^{-1}s^{-1}$)	k_{off} (s^{-1})	$T_{1/2}$ (min)	K_d
IL-22/sIL-22R1[a]	1.4×10^5	2.9×10^{-3}	4.0	20 nM
$sIL\text{-}22R1_{DDQ}$[a]	1.5×10^5	1.9×10^{-3}	6.1	13 nM
$sIL\text{-}22R1_{DDQ}$[b]	1.3×10^6	1.6×10^{-3}	7.4	1 nM
IL-22BPI2	1.3×10^{6}[b]	1.7×10^{-6}[a]	6834	1 pM[c]
IL-22BPI3[b]	6.7×10^5	2.4×10^{-3}	4.8	4 nM
sIL-10R2[d]	-	-	-	120 μM
IL-22:sIL-22R1/sIL-10R2[d]	-	-	-	12 μM
IL-10/sIL-10R1[e]	5.70×10^5	2.60×10^{-4}	44	0.47 nM
sIL-10R2[f]	-	-	-	~mM
IL-10:sIL-10R1/sIL-10R2[g]	-	-	-	234 μM

Affinities in the table are between italicized and nonitalicized components.
[a] Experiments performed on amine-coupled surfaces.
[b] Experiments performed using Ab-captured sIL-22R1 or IL-22BP isoform surfaces.
[c] K_d derived from k_{on} and k_{off} values (k_{off}/k_{on}) determined in different experiments. Reported values in footnotes a–c are the average of two experiments.
[d] From Logsdon et al. (2004).
[e] From Yoon et al. (2006).
[f] From Logsdon et al. (2002).
[g] From Yoon et al. (2005). $T_{1/2} = 0.693/k_{off}$.

(Figure 2). Asparagines Asn-$68^{IL\text{-}22}$ and Asn-$97^{IL\text{-}22}$ were mutated to glutamine to make $IL\text{-}22_{N\text{-}QQ}$, whereas asparagines Asn-$80^{sIL\text{-}22R1}$ and Asn-$87^{sIL\text{-}22R1}$ were replaced by aspartic acids and Thr-$89^{sIL\text{-}22R1}$ was replaced by glutamine to make $sIL\text{-}22R1_{DDQ}$. $IL\text{-}22_{N\text{-}QQ}$ and $sIL\text{-}22R1_{DDQ}$ exhibit essentially the same affinity for one another as their glycosylated counterparts (Table 1), suggesting the $IL\text{-}22_{N\text{-}QQ}$/$sIL\text{-}22R1_{DDQ}$ crystal structure (IL-22/sIL-22R1 throughout the rest of text) accurately reflects the cell-surface IL-22/IL-22R1 complex.

Overall Structure of IL-22/sIL-22R1

IL-22 and sIL-22R1 form a 1:1 complex in the crystal (Figure 2). sIL-22R1 adopts an L-shaped structure orienting its two fibronectin type III (FBNIII) domains (D1 and D2) at approximately right angles to one another. The structure of sIL-22R1 is similar to sIL-10R1 (Josephson et al., 2001), except the D2 domain of sIL-22R1 is rotated by ~20°, relative to sIL-10R1, about an axis parallel to the D2 β strands. Although considerable conformational differences are observed among free IL-22 structures (Nagem et al., 2002; Xu et al., 2005), sIL-22R1-bound IL-22 molecules are essentially identical (root-mean-square deviation [rmsd] = 0.36 Å). The IL-22/sIL-22R1 complex is most similar to one half of the dimeric IL-10/sIL-10R1 complex (Josephson et al., 2001). Upon superposition of IL-22 onto one subunit of the IL-10 dimer (2.7 Å rmsd, 109 atoms), the C termini of sIL-22R1 and sIL-10R1 chains, prior to their entry into the membrane, are separated by ~12 Å (Figure 2C). Despite similar architectures, IL-22/sIL-22R1 does not form an IL-10-like dimeric complex in the crystal lattice.

The IL-22/sIL-22R1 Interface

The IL-22/sIL-22R1 interface consists of five sIL-22R1 loops (L2–L6) located at the interface of the D1 and D2 domains, which

engage IL-22 residues presented on helix A, the AB loop, and helix F (Figures 2 and 3). The interface may be separated into two major contact surfaces, site 1a and site 1b. L2–L4 loops within the D1 domain form contacts in site 1a, while loops L5 and L6, from D2, contact site 1b.

Site 1a contributes ~72% of the total buried surface area and 11 of 12 hydrogen bond/salt bridge interactions in the IL-22/sIL-22R1 complex (Figures 3 and 4; Table 2). The predominant feature of site 1a is the insertion of Tyr-60$^{sIL\text{-}22R1}$ and Gly-61$^{sIL\text{-}22R1}$ into a small cavity on IL-22 created at the intersection of helix F and the AB loop (Figure 2B). The base of the cavity is formed by helix F residues Lys-162$^{IL\text{-}22}$ and Glu-166$^{IL\text{-}22}$, which each form hydrogen bonds to the OH atom of Tyr-60$^{sIL\text{-}22R1}$. Gly-61$^{sIL\text{-}22R1}$ also forms a hydrogen bond with the O atom of Thr-72$^{IL\text{-}22}$ located in the AB loop. The contacts formed by Tyr-60$^{sIL\text{-}22R1}$ and Gly-61$^{sIL\text{-}22R1}$ are identical to those previously described in the IL-10/sIL-10R1 complex for residues Tyr-43$^{sIL\text{-}10R1}$, Gly-44$^{sIL\text{-}10R1}$, Asp-44$^{IL\text{-}10}$, Lys-138$^{IL\text{-}10}$, and Glu-142$^{IL\text{-}10}$. Thus, the major site 1a binding epitope is conserved in IL-22/sIL-22R1 and IL-10/sIL-10R1 complexes (Figure 4).

In contrast to the extensive site 1a interface, IL-22/sIL-22R1 site 1b is very small and distinct from IL-10/sIL-10R1 (Figures 2 and 4). It is made up almost entirely of van der Waals interactions between IL-22 helix F residues, Met-172$^{IL\text{-}22}$ and Arg-175$^{IL\text{-}22}$, and sIL-22R1 L6 residues, Thr-207$^{sIL\text{-}22R1}$ and Trp-208$^{sIL\text{-}22R1}$ (Figures 2B and 4E). Site 1b contains one salt bridge between Lys-44$^{IL\text{-}22}$, located in the preA helix, and Asp-162$^{sIL\text{-}22R1}$, located on the L5 loop.

Mechanisms Regulating IL-22/sIL-22R1 and IL-10/sIL-10R1 Affinity

Using the structures of IL-22/sIL-22R1 and IL-10/sIL-10R1, we sought to explain the distinct binding kinetics of the complexes (Table 1). Our past SPR analysis of IL-22/sIL-22R1 interactions used amine-coupled IL-22, which can prevent the accurate estimation of on-rates (Logsdon et al., 2002, 2004). To test for this possibility, we redesigned our SPR experiment by injecting IL-22 over sIL-22R1-His$_6$ captured on an anti-His$_6$ antibody surface. Using this experimental setup, an on-rate of 1.3×10^6 $M^{-1}s^{-1}$ was obtained for the IL-22/sIL-22R1 interaction, which is an ~9-fold increase over previous amine-coupled experiments and ~6-fold faster than observed for the IL-10/sIL-10R1 interaction (Table 1). Interestingly, the overall affinity of each complex is similar (1 nM versus 0.47 nM), but the occupancy time of the ligand on the receptor, quantified by the complex half-life ($T_{1/2}$), is 7.4 min for IL-22/sIL-22R1 versus 44 min for IL-10/sIL-10R1.

The amounts of buried surface area and specific contacts in the IL-22/IL-22R1 and IL-10/sIL-10R1 complexes are consistent with the observed binding kinetics. The IL-22/sIL-22R1 interface buries 1585 Å^2 of surface compared to 1893 Å^2 for IL-10/sIL-10R1. In both complexes, site 1a forms the predominant contact surface. In IL-22/sIL-22R1, it consists of 1141 Å^2 of buried surface area and 11 of 12 hydrogen bonds identified in the complex (Table 2). Similarly, the IL-10/sIL-10R1 site 1a interface consists of 1249 Å^2 (9% larger than IL-22/sIL-22R1) and forms 10 hydrogen bonds (Yoon et al., 2005).

Larger differences are observed in site 1b, which consists of 444 Å^2 in IL-22/sIL-22R1 compared to 664 Å in IL-10/sIL-10R1 (a 33% difference). In addition, IL-10/sIL-10R1 site 1b contains six hydrogen bonds compared to only one in IL-22/sIL-22R1 (Figures 4E and 4F). As a result, the number of hydrogen bonds per 100 Å^2 of surface area (HB/100 Å) is ~1.7 throughout the entire IL-10/sIL-10R1 site 1 interface. In contrast, IL-22/sIL-22R1 site 1a and 1b interfaces exhibit HB/100 Å values of 1.9 and 0.5, respectively. These comparisons suggest that the reduced size (buried surface area and contacts) of IL-22/sIL-22R1 site 1b is mainly responsible for its faster off-rate compared to IL-10/sIL-10R1.

IL-22/IL-22BP Interactions

To further evaluate the role of site 1a and 1b in IL-22 binding affinity, we studied the binding kinetics of IL-22BP isoforms IL-22BPI2 and IL-22BPI3 for IL-22 (Figure 5; Table 1). Homology models of IL-22/IL-22BPI2 and IL-22/IL-22BPI3 reveal IL-22BPI2 forms site 1a and 1b contacts with IL-22, whereas IL-22BPI3 only forms site 1a contacts. With one exception, the models suggest that all site 1a IL-22/IL-22R1 contacts are conserved in IL-22/IL-22BPI2 and IL-22/IL-22BPI3 complexes (Table 2). Thus, the IL-22/IL-22BPI3 complex essentially mimics an IL-22/sIL-22R1 site 1a interface. Using SPR methods, IL-22/IL-22BPI3 exhibits a dissociation constant (K_d) of ~4 nM compared to 1 nM for the IL-22/sIL-22R1 complex (Figure 5; Table 1). The off-rate of the IL-22/IL-22BPI3 complex (2.4×10^{-3} $M^{-1}s^{-1}$) is only 1.5-fold faster than observed for the IL-22/sIL-22R1 complex. Thus, both the structure analysis (Figure 4E) and SPR data suggest site 1b contributes very little to the overall stability of the IL-22/sIL-22R1 complex.

In contrast to sIL-22R1 and IL-22BPI3, homology modeling of the IL-22/IL-22BPI2 complex suggests that the D2 domain of IL-22BPI2 forms extensive site 1b contacts with IL-22 (Figure 5D). Key features of this interface are five new salt bridge/hydrogen bonds (Table 2) and the formation of a hydrophobic cluster composed of Trp-116$^{IL\text{-}22BPI2}$ and Leu-208$^{IL\text{-}22BPI2}$ and IL-22 residues Phe-57$^{IL\text{-}22}$, Phe-171$^{IL\text{-}22}$, and Met-172$^{IL\text{-}22}$.

Consistent with the homology model, SPR analysis revealed a K_d of ~1 pM, with a $T_{1/2}$ of 4.7 days, for the IL-22/IL-22BPI2 interaction (Table 1). The extremely slow off-rate of the IL-22/IL-22BPI2 complex was determined by a 22 hr SPR experiment that monitored the dissociation of IL-22BPI2 from amine-coupled IL-22 surfaces (Figure 5). Because Asn-54$^{IL\text{-}22}$ makes a putative hydrogen bond with Asp-209$^{IL\text{-}22BPI2}$, we characterized the loss of IL-22BPI2 from amine-coupled surfaces of glycosylated IL-22 (IL-22$_{NNN}$), as well as IL-22 mutants where N-linked carbohydrate attachment residues Asn-54$^{IL\text{-}22}$ (IL-22$_{QNN}$) and Asn-68$^{IL\text{-}22}$ (IL-22$_{NQN}$) were changed to glutamines. Consistent with our model, a total of 8 response elements (RU) of IL-22BPI2 dissociated from amine-coupled IL-22$_{NNN}$ and IL-22$_{NQN}$ in the 22 hr period, whereas 28 RU of IL-22BPI2 dissociated from the IL-22$_{QNN}$ surface, presumably by disrupting the Asn-54$^{IL\text{-}22}$/Asp-209$^{IL\text{-}22BPI2}$ interaction by the glutamine mutation. These studies further infer a link between high-affinity binding of IL-22/IL-22BPI2 and IL-10/sIL-10R1 with the size of site 1b.

Specificity of IL-22/sIL-22R1 and IL-10/IL-10R1 Complexes

IL-22 and IL-10 cellular responses require efficient targeting to specific cells via their high-affinity chains IL-22R1 and IL-10R1. Closer structural analysis revealed that the conserved site 1a

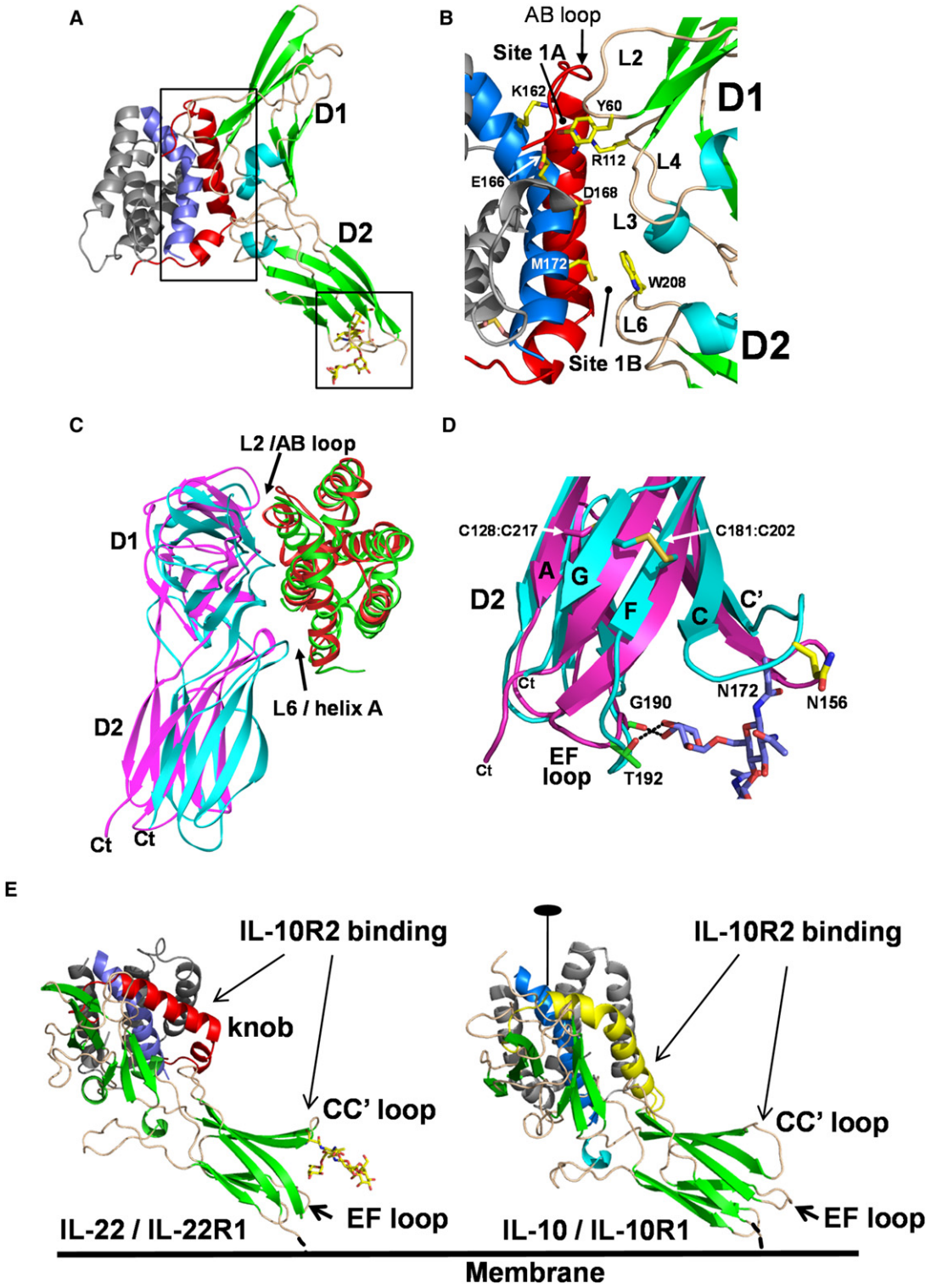

Figure 2. Structure of the IL-22/IL-22R1 Complex

(A) Ribbon diagram of the IL-22/IL-22R1 complex. Helix A/AB loop and helix F that form the sIL-22R1 binding site are colored red and blue, respectively. Boxes show the location of (B) and (E), respectively.

(B) IL-22/sIL-22R1 site 1 interface.

(C) Superposition of IL-22/sIL-22R1 and one half of the IL-10/sIL-10R1 dimer structure. IL-22 is colored red, sIL-22R1 is magenta, IL-10 is green, and sIL-10R1 is cyan.

(D) Structural differences, including the role of carbohydrate, between sIL-22R1 and sIL-10R1 D2 domains.

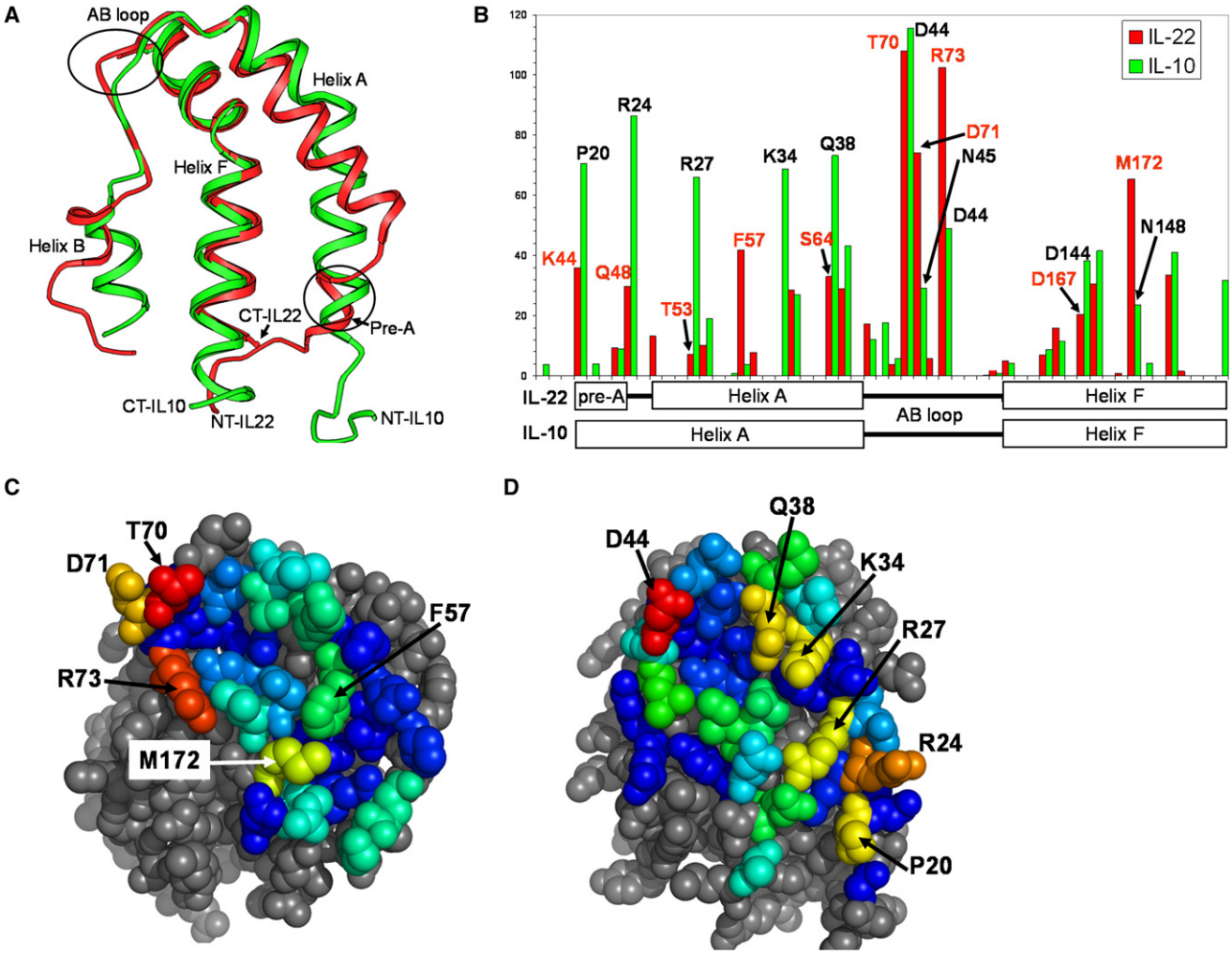

Figure 3. IL-22 and IL-10 Exhibit Distinct Site 1 Structures and Binding Surfaces

(A) Superposition of IL-22 and IL-10 site 1 binding epitopes are colored as described in Figure 2C.

(B–D) Bar graph of IL-22 and IL-10 surface area buried in the site 1 interfaces of IL-22/sIL-22R1 and IL-10/sIL-10R1. Space-filling models are colored according to the amount of surface area buried (red, greatest; dark blue, least) at each residue position in the IL-22 (C) and IL-10 (D) site 1 interfaces.

L2/AB loop recognition motif, which consists of Tyr-60$^{sIL\text{-}22R1}$ and Gly-61$^{sIL\text{-}22R1}$, is a critical specificity determinant (Figure 4). This is because the precise geometry of the hydrogen bonds formed by these residues cannot be accurately reproduced in noncognate complexes (e.g., IL-22/sIL-10R1 or IL-10/sIL-22R1) without steric clashes between other regions of the molecules (Figure 2C).

For example, superposition of IL-22 onto IL-10/sIL-10R1 results in close contacts (~1 Å) between main-chain atoms from the IL-22 preA helix and sIL-10R1 L6 loop, which would prevent complex formation. Likewise, when IL-10 is superimposed onto the IL-22/sIL-22R1 complex, close contacts occur between the AB loop of IL-10 and the L2 loop of sIL-22R1. Proper hydrogen bonding between the IL-10 AB loop and sIL-22R1 L2 loop can be obtained by reorienting IL-10 on the surface of IL-22R1. However, this results in additional disruptions in site 1b located on the other side of the complex. Thus, the requirement for specific contacts in two spatially distinct regions of the interfaces, site 1a and site 1b, provides critical constraints that ensure specificity between the IL-22/IL-22R1 and IL-10/IL-10R1 complexes.

Although essentially the same residues form IL-22/sIL-22R1 and IL-10/IL-10R1 site 1 interfaces, the amount of buried surface area and the number of contacts contributed by each residue are very different (Figure 3). For example, IL-22 AB loop residues Thr-70$^{IL\text{-}22}$ (108 Å^2), Asp-71$^{IL\text{-}22}$ (74 Å^2), and Arg-73$^{IL\text{-}22}$ (102 Å^2) bury the most (>70 Å^2) surface area in the IL-22/sIL-22R1 complex. Asp-44$^{IL\text{-}10}$, which is structurally identical to Thr-70$^{IL\text{-}22}$, buries the most surface area (116 Å^2) of any residue in the IL-10/sIL-10R1 complex. However, IL-10 helix A residues bury large amounts of surface area (Pro-20$^{IL\text{-}10}$, 71 Å^2;

(E) Putative orientation of IL-22/IL-22R1 and IL-10/IL-10R1 cell-surface complexes. The IL-10/IL-10R1 complex is oriented so that the IL-10 dimer twofold axis is perpendicular to the membrane. The helix A/AB loop and helix F residues of IL-10, which form the IL-10R1 binding site, are colored yellow and blue.

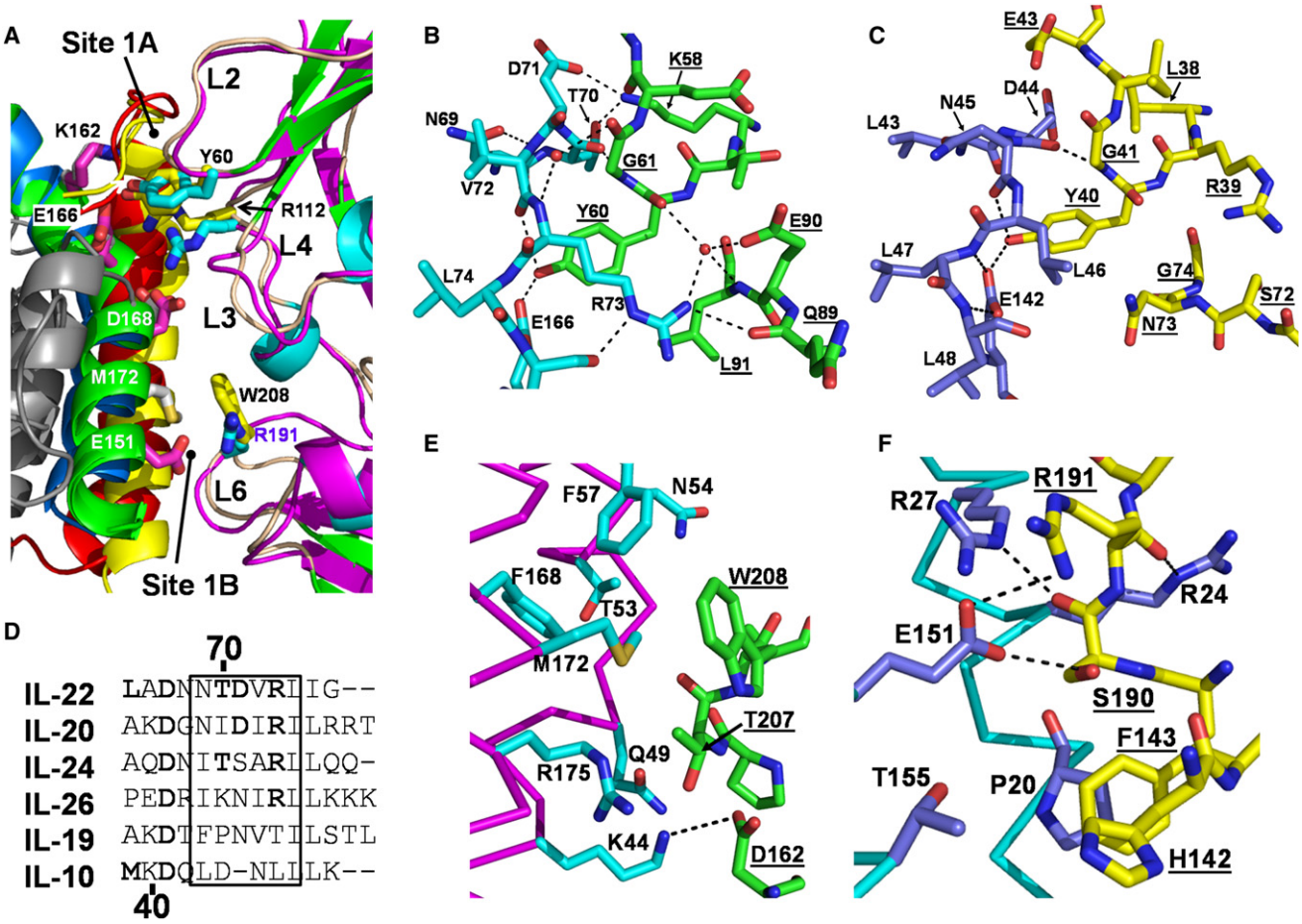

Figure 4. Comparison of IL-22/sIL-22R1 and IL-10/sIL-10R1 Interfaces

(A–C) Enlarged picture of IL-22 and IL-10 site 1 interfaces, as shown in Figure 2A, except the D1 domains of the receptors are superimposed. Important AB loop hydrogen bonds formed in IL-22/sIL-22R1 site 1a (B) and IL-10/sIL-10R1 site 1a (C) are shown.

(D–F) Sequence alignment of IL-10 family cytokine AB loops. Interactions in IL-22/sIL-22R1 site 1b (E) and IL-10/sIL-10R1 site 1b (F) are also shown. Receptor residue labels are distinguished from the ligand labels by underlining.

Arg-24^{IL-10}, 87 Å^2; Arg-27^{IL-10}, 66 Å^2; Lys-34^{IL-10}, 69 Å^2; Gln-38^{IL-10}, 73 Å^2) into sIL-10R1, which is not observed in IL-22/sIL-22R1 (Figure 3).

Because of the extensive interactions made between the IL-22 AB loop and sIL-22R1, including 5 of 12 hydrogen bonds in the interface (Table 2; Figure 3), the AB loop sequences of other IL-10 family members were compared to determine whether these residues were conserved in IL-20 and IL-24, which also bind to IL-22R1. As shown in Figure 4D, IL-20 and IL-24, but not IL-10, IL-19, or IL-26, contain two of the three IL-22 AB loop residues (IL-20, Arg-73^{IL-22} and Asp-71^{IL-22}; IL-24, Arg-73^{IL-22} and Thr-70^{IL-22}), suggesting they are important specificity determinants that promote interactions with IL-22R1.

Promiscuous IL-10R2 Binding to IL-22/IL-22R1 and IL-10/IL-10R1 Complexes

IL-22 and IL-10 both engage the common low-affinity signal transducing chain IL-10R2 (Kotenko et al., 1997, 2001a; Xie et al., 2000). A previous model of the IL-10/IL-10R1/IL-10R2 ternary complex, generated without any biochemical constraints, defined the general location of the IL-10R2 binding site (Pletnev et al., 2005). Here, our goal was to generate models of the IL-22 and IL-10 ternary signaling complexes (TC) that explain the distinct affinities of sIL-10R2 for IL-22/sIL-22R1 (K_d ~14 μM) and IL-10/sIL-10R1 (K_d ~234 μM) binary complexes (Table 1). To accomplish this, we used IL-22/sIL-22R1 and IL-10/sIL-10R1 (Josephson et al., 2001) structures and mutagenesis studies that mapped the IL-10R2 binding sites on IL-10 (Yoon et al., 2006) and on IL-22 (Logsdon et al., 2004) as experimental constraints for TC model generation.

As shown in Figure 6, sIL-10R2 contacts IL-22/sIL-22R1 and IL-10/sIL-10R1 binary complexes at three distinct surfaces labeled sites 2a, 2b, and 2c. Sites 2a and 2b are predominantly between sIL-10R2 and helices A and D of IL-22 and IL-10, whereas receptor D2$^{sIL-10R2}$/D$^{sIL-22R1}$ or D2$^{sIL-10R2}$/D2$^{sIL-10R1}$ interactions make up site 2c. A total of ten hydrogen bond/salt bridge interactions was identified in the IL-22 and IL-10 site 2 interfaces (Table S2). Five of the ten interactions use the same sIL-10R2 residue in both IL-22 and IL-10 TC complexes. The amount of surface area buried by IL-10R2 in the IL-10 TC site

Table 2. Potential Hydrogen Bonds in IL-22/IL-22R1 and IL-22/IL-22BP Complexes

IL-22				IL-22R1								IL-22BPI3[a]			IL-22BPI2[a]			
Number	Location	Residue	Atom	Number	Location	Residue	Atom	L/R	M/S	Average	Site	Number	Residue	Atom	Number	Residue	Atom	**Dist**
44	preA	Lys	NZ	162	L5	Asp	OD2	3.6	3.4	3.5	1b	-	-	-	162	Glu	OE1	3.0
48	preA	Gln	OE1	-	-	-	-	-	-	-	1b	-	-	-	207	Met	N	3.3
54	A	Asn	ND2	-	-	-	-	-	-	-	1b	-	-	-	209	Asp	OD1	3.4
61	A	Lys	NZ	111	L4	Asp	OD2	2.7	3.6	3.2	1a	118	Glu	OE2	118	Glu	OE2	3.6
67	AB	Asp	OD2	112	L4	Arg	NH2	3.6	3.2	3.4	1a	Conserved	Conserved					
70	AB	Thr	O	61	L2	Gly	N	3.1	2.9	3.0	1a	Conserved	Conserved					
70	AB	Thr	OG1	58	L2	Lys	NZ	2.5	3.0	2.8	1a	Conserved	Conserved					
71	AB	Asp	OD1	58	L2	Lys	NZ	2.8	3.0	2.9	1a	Conserved	Conserved					
72	AB	Val	O	60	L2	Tyr	OH	3.3	3.1	3.2	1a	Conserved	Conserved					
73	AB	Arg	NH1	89	L3	Gln	O	3.2	2.7	3.0	1a	Conserved	Conserved					
73	AB	Arg	NH2	89	L3	Gln	O	3.7	3.3	3.5	1a	Conserved	Conserved					
162	F	Lys	NH1	60	L2	Tyr	OH	3.1	2.9	3.0	1a	Conserved	Conserved					
165	F	Gly	O	112	L4	Arg	NH1	3.1	3.6	3.4	1a	Conserved	Conserved					
166	F	Glu	OE2	60	L2	Tyr	OH	2.4	3.0	2.7	1a	Conserved	Conserved					
175	F	Arg	NH1	-	-	-	-	-	-	-	1b	-	-	-	162	Glu	OE1	3.0
175	F	Arg	NH2	-	-	-	-	-	-	-	1b	-	-	-	162	Glu	OE2	2.7

L/R and M/S represent distances observed between the noncrystallographic symmetry-related IL-22/IL-22R1 complexes. "Conserved" denotes contacts found in the IL-22/IL-22R1 and IL-22/IL-22BP models.
[a] IL-22/IL-22BP contacts based on homology models.

2 interface is ~1200 Å^2, which corresponds to an HB/100 Å ratio of ~0.8, which is similar to the IL-22/sIL-22R1 site 1b interface (0.5 HB/100 Å; Figure 4E). The IL-22 TC site 2 interface is smaller (~900 Å^2), resulting in a slightly larger HB/100 Å ratio of ~1.1.

In addition to characterizing the low-affinity binding properties of site 2, the TC models suggest that structural differences in the ligands determine IL-10R2 affinity for IL-22 and IL-10 binary complexes. In the IL-22 TC, the N-terminal end of helix A presents a knob-like surface for interactions with the binding loops of sIL-10R2 (Figure 2E). In contrast, the surface presented by helix A in IL-10 is essentially flat, which is consistent with its lower affinity for IL-10R2. Arg-55^{IL-22} and Arg-32^{IL-10} both form conserved salt-bridge interactions with Asp-84$^{sIL-10R2}$, but structural differences that could alter sIL-10R2 affinity are present. Specifically, the side-chain conformation of Arg-55^{IL-22} is fixed by additional contacts with Tyr-51^{IL-22}, whereas there are no such constraints on Arg-32^{IL-10}. These findings are consistent with the 120 μM affinity of the IL-22/IL-10R2 interaction compared to the ~mM affinity of the IL-10/IL-10R2 interaction (Table 1).

The most extensive contacts in the IL-10 TC are observed in site 2b, which consists of the tripartite interaction between Arg-24^{IL-10}, the L6 loop of sIL-10R1, and Asn-147$^{sIL-10R2}$. In a manner similar to the presentation of Arg-55^{IL-22} on the knob of IL-22, sIL-10R1 interactions with Arg-24^{IL-10} orient the side chain for interactions with Asn-147$^{sIL-10R2}$. The most diverse contacts in the IL-22 and IL-10 TCs occur in site 2c. In particular, Glu-121$^{sIL-10R2}$ forms a hydrogen bond with Ser-174$^{sIL-10R1}$ in the IL-10 TC. However, in the IL-22 TC, Glu-121$^{sIL-10R2}$ interacts with the N-acetylglucosamine attached to Asn-174$^{sIL-22R1}$ (Figures 2D, 2E, and 6). This is especially interesting because previous characterization of IL-22/sIL-10R2 interactions found carbohydrate attached to Asn-54^{IL-22} to be important for sIL-10R2 binding (Logsdon et al., 2004).

DISCUSSION

IL-22 folds into a compact monomeric structure, in contrast to IL-10, which assembles into domain-swapped dimers (Nagem et al., 2002; Walter and Nagabhushan, 1995; Xu et al., 2005; Zdanov et al., 1995). Interestingly, recent X-ray scattering data revealed that IL-22 forms noncovalent dimers, and tetramers, in solution that adopt V-shaped structures similar to the IL-10 dimer (de Oliveira Neto et al., 2008). Although we do not observe an IL-10-like dimer complex in the crystal lattice, it is clear that IL-22 and IL-10 form receptor complexes with very similar architectures. This suggests that the overall receptor complex structure, with the exception of oligomerization (e.g., monomer/dimer transition), is not responsible for differences in IL-22 and IL-10 signaling.

FRET data have revealed that IL-10R1 and IL-10R2 associate with one another on the cell surface in the absence of IL-10 (Krause et al., 2006). Because IL-22R1 pairs with IL-10R2 to induce IL-22 signaling, IL-22R1 and IL-10R2 are also predicted to form cell-surface heterodimers (Krause et al., 2006). Based on mechanistic studies of growth hormone and erythropoietin signaling, binding of IL-22 and IL-10 to their respective R1/R2 heterodimers is expected to induce rotational and/or conformational changes in the receptors leading to cell signaling (Brown et al., 2005; Remy et al., 1999). Although many of the general features of the IL-22 and IL-10 signaling complexes are conserved, IL-22 and IL-10 exhibit unique specificities and receptor binding kinetics, which are dependent on the structural details of the site 1 and site 2 interfaces. IL-22/IL-22R1 and IL-10/IL-10R1 site 1 contacts exhibit K_d values (nM) that are at least four orders of magnitude higher than site 2 contacts made by the common IL-10R2 chain (μM).

Because of the large differences in the site 1 and site 2 binding affinity/kinetics, IL-22 and IL-10 TC activation are R1 dominant.

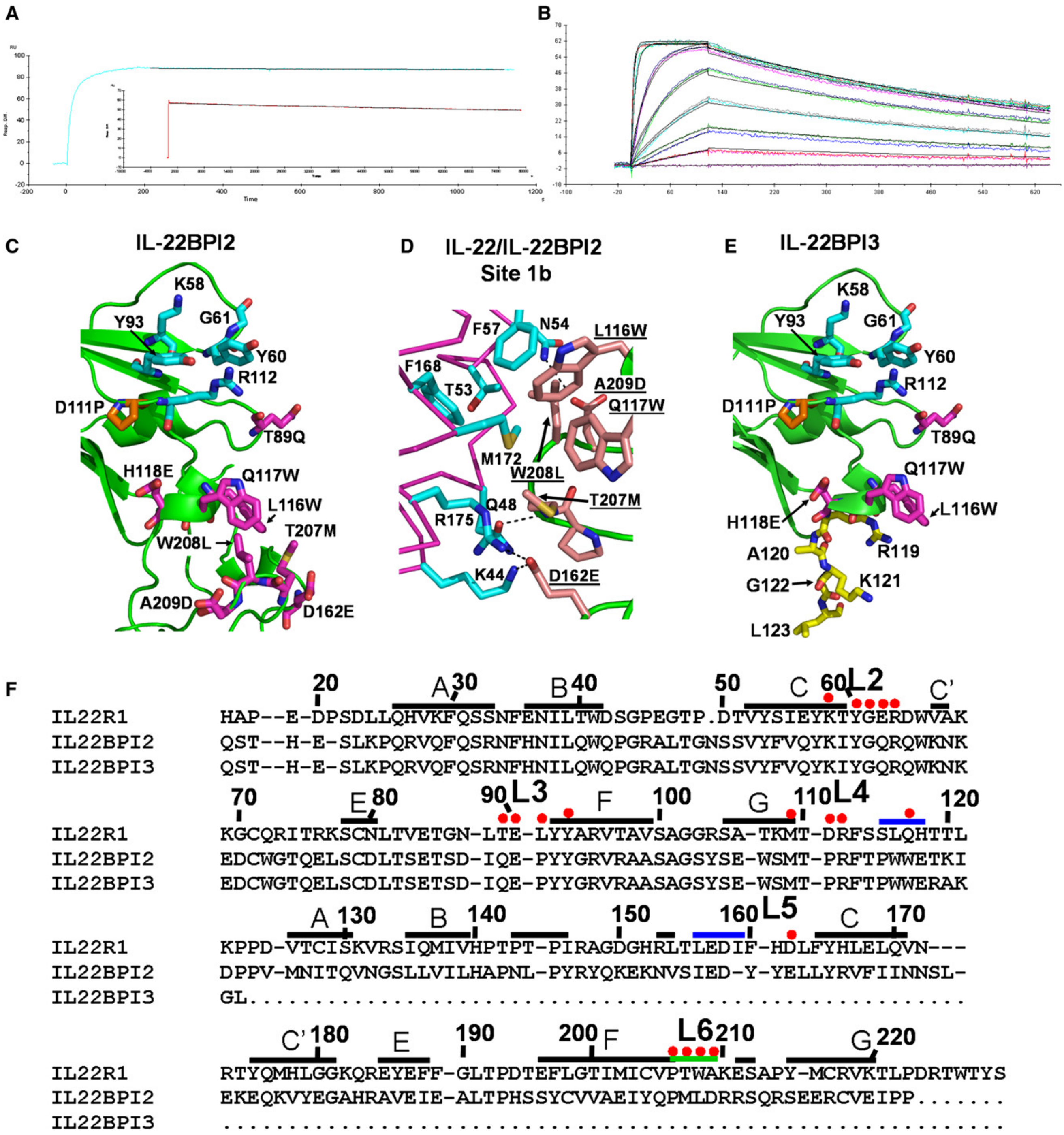
A
B
C IL-22BPI2
D IL-22/IL-22BPI2 Site 1b
E IL-22BPI3
F
IL22R1 HAP--E-DPSDLLQHVKFQSSNFENILTWDSGPEGTP.DTVYSIEYKTYGERDWVAK
IL22BPI2 QST--H-E-SLKPQRVQFQSRNFHNILQWQPGRALTGNSSVYFVQYKIYGQRQWKNK
IL22BPI3 QST--H-E-SLKPQRVQFQSRNFHNILQWQPGRALTGNSSVYFVQYKIYGQRQWKNK
IL22R1 KGCQRITRKSCNLTVETGN-LTE-LYYARVTAVSAGGRSA-TKMT-DRFSSLQHTTL
IL22BPI2 EDCWGTQELSCDLTSETSD-IQE-PYYGRVRAASAGSYSE-WSMT-PRFTPWWETKI
IL22BPI3 EDCWGTQELSCDLTSETSD-IQE-PYYGRVRAASAGSYSE-WSMT-PRFTPWWERAK
IL22R1 KPPD-VTCISKVRSIQMIVHPTPT-PIRAGDGHRLTLEDIF-HDLFYHLELQVN---
IL22BPI2 DPPV-MNITQVNGSLLVILHAPNL-PYRYQKEKNVSIED-Y-YELLYRVFIINNSL-
IL22BPI3 GL.
IL22R1 RTYQMHLGGKQREYEFF-GLTPDTEFLGTIMICVPTWAKESAPY-MCRVKTLPDRTWTYS
IL22BPI2 EKEQKVYEGAHRAVEIE-ALTPHSSYCVVAEIYQPMLDRRSQRSEERCVEIPP.
IL22BPI3 .

Figure 5. Binding and Structure of IL-22BP Isoforms

(A) Short (7 min) and long (22 hr, inset) period sensorgrams used to derive the affinity of the IL-22/IL-22BPI2 interaction (see Table 1).

(B) Sensorgram performed using IL-22BPI3-His$_6$ captured to anti-His Ab surfaces, followed by the injection of IL-22. Larger versions of the sensorgram are shown in Figure S1.

(C) Homology model of IL-22BPI2 colored to show the location of residue differences and similarities with sIL-22R1. Residues conserved between IL-22BPI2 and sIL-22R1 are colored cyan, and differences are colored magenta. The orange residue, Pro-111$^{\text{IL-22BP}}$, highlights the one amino change in D1 that alters contacts with IL-22.

(D) Site 1b interface observed in the IL-22/IL-22BPI2 homology model.

(E) Model of the IL-22BPI3 colored as described in (C). Unique C-terminal residues of IL-22BPI3 are shown in yellow.

(F) Sequence alignment of sIL-22R1 and IL-22BP isoforms. sIL-22R1 residues that bind IL-22 are labeled with red dots.

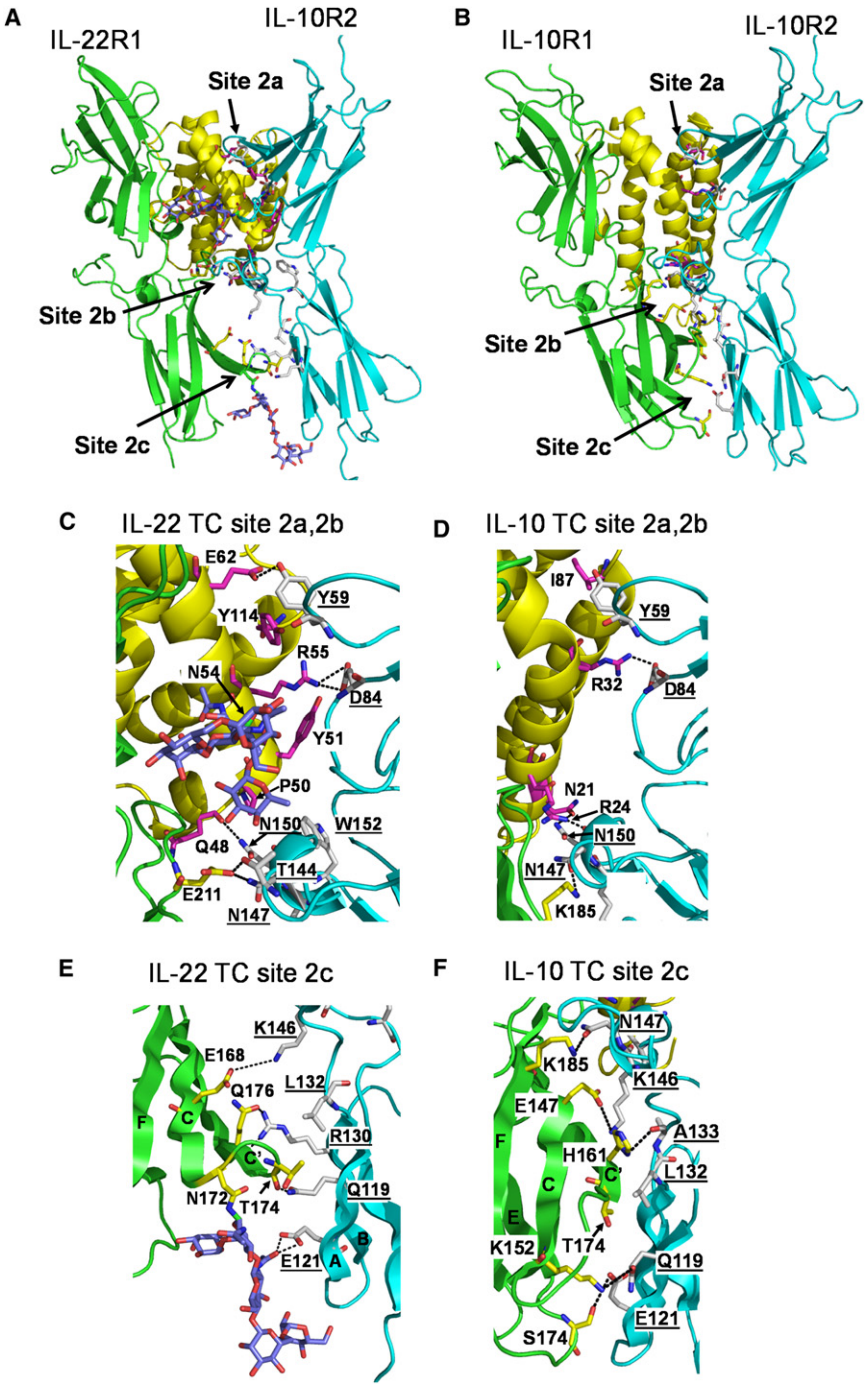

Figure 6. Models of the IL-22/IL-22R1/IL-10R2 and IL-10/IL-10R1/IL-10R2 Ternary Complexes

Overall IL-22 (A) and IL-10 (B) ternary complex structures. Enlarged pictures of the IL-22 (C) and IL-10 (D) site 2a/2b and IL-22 (E) and IL-10 (F) site 2c are also shown.

This suggests that despite the preassociation of R1 and R2 chains on the cell surface, cell specificity/targeting and receptor occupancy time are controlled by the binding kinetics of the R1 chains, which are selectively expressed on different cell types (Nagalakshmi et al., 2004). In contrast to IL-22R1 and IL-10R1, IL-10R2 is ubiquitously expressed on all cell types (Nagalakshmi et al., 2004). The weak binding of IL-10R2, via site 2, suggests that it functions as a sensor chain which activates signaling based on the kinetics of the R1 chain, via site 1. Weak site 2 binding also promotes promiscuous IL-10R2 interactions with IL-22, IL-10, and other cytokines (IL-26, IL-28, and IL-29), and reduces the number of unique chains required for IL-10 family cytokine signaling. Our conclusions, based on SPR data, agree with IL-10 cell-surface binding studies that reveal that IL-10 binds to cells expressing only the IL-10R1 chain with an identical affinity as cells expressing both IL-10R1 and IL-10R2 (Ding et al., 2001).

Additional regulation of IL-22 cell targeting/signaling is suggested by the structure and binding properties of IL-22BP isoforms. Our analysis suggests that IL-22/IL-22BPI2 forms an extremely tight (K_d ~1 pM) interaction with IL-22, which differs considerably from the 1 nM K_d obtained by another recent SPR analysis of the IL-22/IL-22BPI2 complex (Wolk et al., 2007). Possible reasons for these discrepancies are the use of amine-coupled IL-22 by Wolk et al., which can lead to reduced on-rates, and the use of short dissociation times, which can underestimate slow off-rates. Also in contrast to Wolk et al., our capture experiments suggest that sIL-22R1 and IL-22BPI2 exhibit essentially identical on-rates. However, the off-rates differ dramatically, resulting in $T_{1/2}$ values of ~7 min for IL-22/sIL-22R1 compared to ~4.7 days for IL-22/IL-22BP. The impact of these findings on IL-22 biology depends on IL-22, IL-22R1, and IL-22BP levels in various tissues, which are now being explored in more detail.

SPR analysis of IL-22BPI3 reveals that it displays binding kinetics similar to the IL-22/sIL-22R1 complex. Analysis of IL-22BPI3 confirms the importance of site 1a for IL-22 binding and the small role of site 1b in IL-22/sIL-22R1 interactions. The functional role of the IL-22BPI3 isoforms remains unclear. Relative to IL-22BPI2, IL-22BPI3 is essentially inactive due to an ~2800-fold reduction in IL-22 affinity, which suggests splicing may be a mechanism to inactivate IL-22BPI2. However, because IL-22BPI3 does retain sIL-22R1-like affinity for IL-22, it is formally possible that IL-22/IL-22BPI3 complexes have a yet unknown role in IL-22 biology.

In addition to providing a structural model that explains observed IL-10R2 affinities and promiscuity, the IL-22 TC model

has also revealed a possible role for N-linked glycosylation in IL-22R1/IL-10R2 site 2c interactions. This is interesting because carbohydrate attached to IL-22 (Asn-54^{IL-22}) was previous shown to be important for IL-10R2 binding (Logsdon et al., 2004). Docking studies were performed in the presence of Asn-54^{IL-22}-linked carbohydrate obtained from the crystal structure of glycosylated IL-22 (Xu et al., 2005). Thus, the IL-22 TC contains sufficient space to accommodate N-linked carbohydrate between sIL-22R1 and sIL-10R2, but an explanation for how mutation of Asn-54^{IL-22} to glutamine disrupts sIL-10R2 binding and cell signaling could not be identified (Logsdon et al., 2004). This may be due to errors in the modeled sIL-10R2 loops, or Asn-54^{IL-22} may play an indirect role (e.g., mediate conformational changes) in activating the IL-22 TC.

In addition to IL-22 signaling complexes, IL-22R1 along with IL-20R2 also form promiscuous IL-20 and IL-24 TCs. However, IL-20/sIL-22R1 interactions are weak, based on our inability to isolate a stable IL-20/sIL-22R1 complex by size-exclusion chromatography (N.J.L. and M.R.W., unpublished results). Thus, in contrast to the R1-dominant IL-22 and IL-10 signaling complexes, sIL-22R1 appears to play a different role in IL-20 and IL-24 complexes. We have identified two critical recognition elements that facilitate promiscuous binding by IL-22R1. First, IL-20 and IL-24 conserve two of three IL-22 AB loop residues (Thr-70^{IL-22}, Asp-71^{IL-22}, and Arg-73^{IL-22}) that form extensive contacts with sIL-22R1. Second, the low affinity of IL-20/sIL-22R1 is consistent with the small site 1b interface observed in IL-22/sIL-22R1, which in our specificity model is critical for promiscuous contacts. The necessity of these affinity and specificity differences may allow fine-tuning of IL-19, IL-20, and IL-24 signaling via IL-22R1/IL-20R1 versus IL-20R1/IL-20R2 complexes in the skin compared to other tissues. The detailed structural basis that regulates these distinct signaling mechanisms will be the focus of future investigations.

EXPERIMENTAL PROCEDURES

Crystallization, Data Collection, and Structure Determination

Crystals of the IL-22/sIL-22R1 complex were obtained as described by Jones et al. (2008). X-ray diffraction data were collected at the Southeast Regional Collaborative Access Team (SER-CAT) 22-ID beamline at the Advanced Photon Source, Argonne National Laboratory, Argonne, Illinois. The structure of the IL-22/sIL-22R1 complex was solved by molecular replacement, using MOLREP (CCP4, 1994) and SAD phasing methods implemented in CNS version 1.1 (Brunger et al., 1998). The sIL-22R1 model was built using O (Jones et al., 1991). Buried surface area was calculated using NACCESS (Hubbard and Thorton, 1993). Structural alignments were performed using STAMP (Russell and Barton, 1992) implemented in VMD (Humphrey et al., 1996). Figures were made using Ribbons and PyMOL (Carson, 1997; DeLano, 2002).

Modeling

IL-22BP and IL-10R2 models were made using MODELER version 8.1 (Eswar et al., 2003). sIL-22R1 and IL-10R1 were used as the structural templates for IL-22BP and IL-10R2 model generation, respectively, using the sequence alignments shown in Figure 5 and Figure S2. sIL-10R2 docking was performed manually using PyMOL (DeLano, 2002) such that IL-10R2 exhibited essentially identical positions in the IL-22 and IL-10 TC complexes and was consistent with major findings of the mutagenesis data (Logsdon et al., 2004; Yoon et al., 2006).

SPR Analysis

SPR experiments were performed on a Biacore 2000 system at 20°C using an HBS running buffer containing 10 mM HEPES (pH 7.4), 0.15 M NaCl, and 0.005% P20 (Biacore). SPR capture experiments were performed by amine coupling 4000 RU of anti-His monoclonal antibody (PHAb; 150 mM NaCl, 20 mM Tris [pH 8]; PentaHis, QIAGEN) on CM-5 research-grade surfaces. C-terminal His_6 constructs sIL-22R1, sIL-22R1$_{DDQ}$, IL-22BPI2, or IL-22BPI3, expressed as described by Logsdon et al. (2004), were injected over the PHAb surface until a total of 120 RU had been captured. Ten different concentrations of IL-22, including a buffer control, were injected over the sIL-22R1, IL-22BPI2, or IL-22BPI3 surfaces in random order at 50 μl/min for 2 min and the dissociation phase was monitored for 7.5 min. Following each IL-22 injection, the PHab surface was cleaned with 0.1 M glycine, 0.5 M NaCl (pH 4.0) followed by fresh receptor and/or binding protein. Reproducible capture was monitored by pre- and postcapture report points, which varied by less than 5 RU. The response curves were globally fit using BIAevaluation version 3.2, which gave equivalent parameters to data analysis using CLAMP version 3.1 (Myszka and Morton, 1998). IL-22BPI2 off-rates were measured as previously described by Logsdon et al. (2004) except the chip surfaces were saturated by injecting 1 μM IL-22BPI2 (2 min contact time) at 50 μl/min and dissociation was followed using a data collection rate of 1 point per 10 s for 22 hr.

ACCESSION NUMBERS

Coordinates and structure factors of the IL-22/sIL-22R1 complex have been deposited in the Protein Data Bank under ID code 3DGC.

SUPPLEMENTAL DATA

Supplemental Data include two figures and two tables and can be found with this article online at http://www.structure.org/cgi/content/full/16/9/1333/DC1/.

ACKNOWLEDGMENTS

Use of the Advanced Photon Source (SER-CAT ID-22) was supported by the U.S. Department of Energy, Office of Science, Office of Basic Energy Sciences, under contract W-31-109-Eng-38. This work was funded by grant AI047300 from the NIH.

Received: April 18, 2008
Revised: June 13, 2008
Accepted: June 19, 2008
Published online: July 3, 2008

REFERENCES

Aujla, S.J., Chan, Y.R., Zheng, M., Fei, M., Askew, D.J., Pociask, D.A., Reinhart, T.A., McAllister, F., Edeal, J., Gaus, K., et al. (2008). IL-22 mediates mucosal host defense against Gram-negative bacterial pneumonia. Nat. Med. *14*, 275–281.

Blumberg, H., Conklin, D., Xu, W.F., Grossmann, A., Brender, T., Carollo, S., Eagan, M., Foster, D., Haldeman, B.A., Hammond, A., et al. (2001). Interleukin 20: discovery, receptor identification, and role in epidermal function. Cell *104*, 9–19.

Boniface, K., Guignouard, E., Pedretti, N., Garcia, M., Delwail, A., Bernard, F.X., Nau, F., Guillet, G., Dagregorio, G., Yssel, H., et al. (2007). A role for T cell-derived interleukin 22 in psoriatic skin inflammation. Clin. Exp. Immunol. *150*, 407–415.

Brown, R.J., Adams, J.J., Pelekanos, R.A., Wan, Y., McKinstry, W.J., Palethorpe, K., Seeber, R.M., Monks, T.A., Eidne, K.A., Parker, M.W., et al. (2005). Model for growth hormone receptor activation based on subunit rotation within a receptor dimer. Nat. Struct. Mol. Biol. *12*, 814–821.

Brunger, A.T., Adams, P.D., Clore, G.M., DeLano, W.L., Gros, P., Grosse-Kunstleve, R.W., Jiang, J.S., Kuszewski, J., Nilges, M., Pannu, N.S., et al. (1998). Crystallography & NMR system: a new software suite for macromolecular structure determination. Acta Crystallogr. D Biol. Crystallogr. *54*, 905–921.

Carson, M. (1997). Ribbons. Methods Enzymol. *277*, 493–505.

CCP4 (Collaborative Computational Project, Number 4) (1994). The CCP4 suite: programs for protein crystallography. Acta Crystallogr. D Biol. Crystallogr. *50*, 760–763.

DeLano, W.L. (2002). PyMOL (http://www.pymol.org/).

de Oliveira Neto, M., Ferreira Junior, J.R., Colau, D., Fischer, H., Nascimento, A.S., Craievich, A.F., Dumoutier, L., Renauld, J.C., and Polikarpov, I. (2008). Interleukin-22 forms dimers that are recognized by two interleukin-22R1 receptor chains. Biophys. J. *94*, 1754–1765.

Ding, Y., Qin, L., Zamarin, D., Kotenko, S.V., Pestka, S., Moore, K.W., and Bromberg, J.S. (2001). Differential IL-10R1 expression plays a critical role in IL-10-mediated immune regulation. J. Immunol. *167*, 6884–6892.

Dumoutier, L., Louahed, J., and Renauld, J.C. (2000a). Cloning and characterization of IL-10-related T cell-derived inducible factor (IL-TIF), a novel cytokine structurally related to IL-10 and inducible by IL-9. J. Immunol. *164*, 1814–1819.

Dumoutier, L., Van Roost, E., Colau, D., and Renauld, J.C. (2000b). Human interleukin-10-related T cell-derived inducible factor: molecular cloning and functional characterization as an hepatocyte-stimulating factor. Proc. Natl. Acad. Sci. USA *97*, 10144–10149.

Dumoutier, L., Leemans, C., Lejeune, D., Kotenko, S.V., and Renauld, J.C. (2001a). Cutting edge: STAT activation by IL-19, IL-20 and mda-7 through IL-20 receptor complexes of two types. J. Immunol. *167*, 3545–3549.

Dumoutier, L., Lejeune, D., Colau, D., and Renauld, J.C. (2001b). Cloning and characterization of IL-22 binding protein, a natural antagonist of IL-10-related T cell-derived inducible factor/IL-22. J. Immunol. *166*, 7090–7095.

Eswar, N., John, B., Mirkovic, N., Fiser, A., Ilyin, V.A., Pieper, U., Stuart, A.C., Marti-Renom, M.A., Madhusudhan, M.S., Yerkovich, B., et al. (2003). Tools for comparative protein structure modeling and analysis. Nucleic Acids Res. *31*, 3375–3380.

Hubbard, S.J., and Thorton, J.M. (1993). NACCESS (computer program). Department of Biochemistry and Molecular Biology, University College London.

Humphrey, W., Dalke, A., and Schulten, K. (1996). VMD: visual molecular dynamics. J. Mol. Graph. *14*, 33–38, 27–28.

Jones, B.C., Logsdon, N.J., and Walter, M.R. (2008). Crystallization and preliminary X-ray diffraction analysis of human IL-22 bound to the extracellular IL-22R1 chain. Acta Crystallogr. Sect. F Struct. Biol. Cryst. Commun. *64*, 266–269.

Jones, T.A., Zou, J.Y., Cowan, S.W., and Kjeldgaard, M. (1991). Improved methods for building protein models in electron density maps and the location of errors in these models. Acta Crystallogr. A *47*, 110–119.

Josephson, K., Logsdon, N.J., and Walter, M.R. (2001). Crystal structure of the IL-10/IL-10R1 complex reveals a shared receptor binding site. Immunity *15*, 35–46.

Kotenko, S.V., Krause, C.D., Izotova, L.S., Pollack, B.P., Wu, W., and Pestka, S. (1997). Identification and functional characterization of a second chain of the interleukin-10 receptor complex. EMBO J. *16*, 5894–5903.

Kotenko, S.V., Izotova, L.S., Mirochnitchenko, O.V., Esterova, E., Dickensheets, H., Donnelly, R.P., and Pestka, S. (2001a). Identification of the functional interleukin-22 (IL-22) receptor complex: the IL-10R2 chain (IL-10Rβ) is a common chain of both the IL-10 and IL-22 (IL-10-related T cell-derived inducible factor, IL-TIF) receptor complexes. J. Biol. Chem. *276*, 2725–2732.

Kotenko, S.V., Izotova, L.S., Mirochnitchenko, O.V., Esterova, E., Dickensheets, H., Donnelly, R.P., and Pestka, S. (2001b). Identification, cloning, and characterization of a novel soluble receptor that binds IL-22 and neutralizes its activity. J. Immunol. *166*, 7096–7103.

Krause, C.D., Mei, E., Mirochnitchenko, O., Lavnikova, N., Xie, J., Jia, Y., Hochstrasser, R.M., and Pestka, S. (2006). Interactions among the components of the interleukin-10 receptor complex. Biochem. Biophys. Res. Commun. *340*, 377–385.

Kunz, S., Wolk, K., Witte, E., Witte, K., Doecke, W.D., Volk, H.D., Sterry, W., Asadullah, K., and Sabat, R. (2006). Interleukin (IL)-19, IL-20 and IL-24 are produced by and act on keratinocytes and are distinct from classical ILs. Exp. Dermatol. *15*, 991–1004.

Lejeune, D., Dumoutier, L., Constantinescu, S., Kruijer, W., Schuringa, J.J., and Renauld, J.C. (2002). Interleukin-22 (IL-22) activates the JAK/STAT, ERK, JNK, and p38 MAP kinase pathways in a rat hepatoma cell line: pathways that are shared with and distinct from IL-10. J. Biol. Chem. *277*, 33676–33682.

Liang, S.C., Tan, X.Y., Luxenberg, D.P., Karim, R., Dunussi-Joannopoulos, K., Collins, M., and Fouser, L.A. (2006). Interleukin (IL)-22 and IL-17 are coexpressed by Th17 cells and cooperatively enhance expression of antimicrobial peptides. J. Exp. Med. *203*, 2271–2279.

Logsdon, N.J., Jones, B.C., Josephson, K., Cook, J., and Walter, M.R. (2002). Comparison of interleukin-22 and interleukin-10 soluble receptor complexes. J. Interferon Cytokine Res. *22*, 1099–1112.

Logsdon, N.J., Jones, B.C., Allman, J.C., Izotova, L., Schwartz, B., Pestka, S., and Walter, M.R. (2004). The IL-10R2 binding hot spot on IL-22 is located on the N-terminal helix and is dependent on N-linked glycosylation. J. Mol. Biol. *342*, 503–514.

Ma, H.L., Liang, S., Li, J., Napierata, L., Brown, T., Benoit, S., Senices, M., Gill, D., Dunussi-Joannopoulos, K., Collins, M., et al. (2008). IL-22 is required for Th17 cell-mediated pathology in a mouse model of psoriasis-like skin inflammation. J. Clin. Invest. *118*, 597–607.

Moore, K.W., de Waal Malefyt, R., Coffman, R.L., and O'Garra, A. (2001). Interleukin-10 and the interleukin-10 receptor. Annu. Rev. Immunol. *19*, 683–765.

Myszka, D.G., and Morton, T.A. (1998). CLAMP: a biosensor kinetic data analysis program. Trends Biochem. Sci. *23*, 149–150.

Nagalakshmi, M.L., Murphy, E., McClanahan, T., and de Waal Malefyt, R. (2004). Expression patterns of IL-10 ligand and receptor gene families provide leads for biological characterization. Int. Immunopharmacol. *4*, 577–592.

Nagem, R.A., Colau, D., Dumoutier, L., Renauld, J.C., Ogata, C., and Polikarpov, I. (2002). Crystal structure of recombinant human interleukin-22. Structure *10*, 1051–1062.

Pestka, S., Krause, C.D., Sarkar, D., Walter, M.R., Shi, Y., and Fisher, P.B. (2004). Interleukin-10 and related cytokines and receptors. Annu. Rev. Immunol. *22*, 929–979.

Pletnev, S., Magracheva, E., Wlodawer, A., and Zdanov, A. (2005). A model of the ternary complex of interleukin-10 with its soluble receptors. BMC Struct. Biol. *5*, 10.

Radaeva, S., Sun, R., Pan, H.N., Hong, F., and Gao, B. (2004). Interleukin 22 (IL-22) plays a protective role in T cell-mediated murine hepatitis: IL-22 is a survival factor for hepatocytes via STAT3 activation. Hepatology *39*, 1332–1342.

Remy, I., Wilson, I.A., and Michnick, S.W. (1999). Erythropoietin receptor activation by a ligand-induced conformation change. Science *283*, 990–993.

Russell, R.B., and Barton, G.J. (1992). Multiple protein sequence alignment from tertiary structure comparison: assignment of global and residue confidence levels. Proteins *14*, 309–323.

Sa, S.M., Valdez, P.A., Wu, J., Jung, K., Zhong, F., Hall, L., Kasman, I., Winer, J., Modrusan, Z., Danilenko, D.M., et al. (2007). The effects of IL-20 subfamily cytokines on reconstituted human epidermis suggest potential roles in cutaneous innate defense and pathogenic adaptive immunity in psoriasis. J. Immunol. *178*, 2229–2240.

Walter, M.R., and Nagabhushan, T.L. (1995). Crystal structure of interleukin 10 reveals an interferon γ-like fold. Biochemistry *34*, 12118–12125.

Wei, C.C., Ho, T.W., Liang, W.G., Chen, G.Y., and Chang, M.S. (2003). Cloning and characterization of mouse IL-22 binding protein. Genes Immun. *4*, 204–211.

Wolk, K., Kunz, S., Witte, E., Friedrich, M., Asadullah, K., and Sabat, R. (2004). IL-22 increases the innate immunity of tissues. Immunity *21*, 241–254.

Wolk, K., Witte, E., Wallace, E., Docke, W.D., Kunz, S., Asadullah, K., Volk, H.D., Sterry, W., and Sabat, R. (2006). IL-22 regulates the expression of genes responsible for antimicrobial defense, cellular differentiation, and mobility in keratinocytes: a potential role in psoriasis. Eur. J. Immunol. *36*, 1309–1323.

Wolk, K., Witte, E., Hoffmann, U., Doecke, W.D., Endesfelder, S., Asadullah, K., Sterry, W., Volk, H.D., Wittig, B.M., and Sabat, R. (2007). IL-22 induces lipopolysaccharide-binding protein in hepatocytes: a potential systemic role of IL-22 in Crohn's disease. J. Immunol. *178*, 5973–5981.

Xie, M.H., Aggarwal, S., Ho, W.H., Foster, J., Zhang, Z., Stinson, J., Wood, W.I., Goddard, A.D., and Gurney, A.L. (2000). Interleukin (IL)-22, a novel human

cytokine that signals through the interferon receptor-related proteins CRF2–4 and IL-22R. J. Biol. Chem. *275*, 31335–31339.

Xu, T., Logsdon, N.J., and Walter, M.R. (2005). Structure of insect-cell-derived IL-22. Acta Crystallogr. D Biol. Crystallogr. *61*, 942–950.

Xu, W., Presnell, S.R., Parrish-Novak, J., Kindsvogel, W., Jaspers, S., Chen, Z., Dillon, S.R., Gao, Z., Gilbert, T., Madden, K., et al. (2001). A soluble class II cytokine receptor, IL-22RA2, is a naturally occurring IL-22 antagonist. Proc. Natl. Acad. Sci. USA *98*, 9511–9516.

Yoon, S.I., Jones, B.C., Logsdon, N.J., and Walter, M.R. (2005). Same structure, different function: crystal structure of the Epstein-Barr virus IL-10 bound to the soluble IL-10R1 chain. Structure *13*, 551–564.

Yoon, S.I., Logsdon, N.J., Sheikh, F., Donnelly, R.P., and Walter, M.R. (2006). Conformational changes mediate interleukin-10 receptor 2 (IL-10R2) binding to IL-10 and assembly of the signaling complex. J. Biol. Chem. *281*, 35088–35096.

Zdanov, A., Schalk-Hihi, C., Gustchina, A., Tsang, M., Weatherbee, J., and Wlodawer, A. (1995). Crystal structure of interleukin-10 reveals the functional dimer with an unexpected topological similarity to interferon γ. Structure *3*, 591–601.

Zenewicz, L.A., Yancopoulos, G.D., Valenzuela, D.M., Murphy, A.J., Karow, M., and Flavell, R.A. (2007). Interleukin-22 but not interleukin-17 provides protection to hepatocytes during acute liver inflammation. Immunity *27*, 647–659.

Zheng, Y., Valdez, P.A., Danilenko, D.M., Hu, Y., Sa, S.M., Gong, Q., Abbas, A.R., Modrusan, Z., Ghilardi, N., de Sauvage, F.J., et al. (2008). Interleukin-22 mediates early host defense against attaching and effacing bacterial pathogens. Nat. Med. *14*, 282–289.

